ACS APPLIED MATERIALS & INTERFACES

www.acsami.org

Research Article

Stretchable Heterogeneous Polymer Networks of High Adhesion and Low Hysteresis

Ping Zhang, Weiyu Zhou, Yunfeng He, Ziyi Xu, Maochun Li, Wei Hong,* and Canhui Yang*

Cite This: https://doi.org/10.1021/acsami.2c12658

Read Online

ACCESS | Metrics & More | Article Recommendations | Supporting Information

ABSTRACT: Adhesives are ubiquitous, but the mutual exclusion between hyperelasticity and adhesiveness impedes their uses in emerging techniques such as flexible/stretchable electronics. Herein, we propose a strategy to synthesize hyperelastic adhesives (HEAs), by designating hyperelasticity and adhesiveness to the bulk and the surface of a polymer network, respectively. The bulk is hyperelastic but nonadhesive, and the surface is viscoelastic but adhesive, while the HEA is hyperelastic and adhesive. We exemplify the principle by synthesizing poly(butyl acrylate) as the bulk and poly(butyl acrylate-*co*-isobornyl acrylate) as the surface. The resulting HEA exhibits a low hysteresis of 4% at 100% strain and an adhesion energy of 270 J m^{-2}. Moreover, the HEA is optically transparent, thermally stable, spontaneously adhesive to various materials, and mechanically stable against cyclic load, relaxation, and creep. We demonstrate two applications enabled by the unique combination of hyperelasticity and adhesiveness. The proposed strategy is generic, paving new avenues for stretchable yet resilient adhesives for diverse applications.

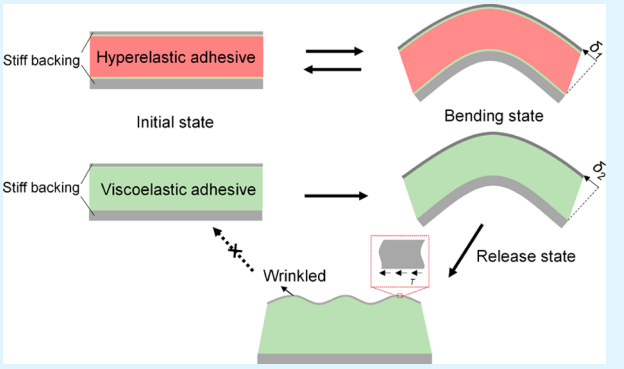

KEYWORDS: *polymer networks, stretchability, heterogeneity, adhesion, low hysteresis*

INTRODUCTION

Adhesives, natural or synthetic, are ubiquitously used to bind different items together and resist their separation.[1] The burgeoning flexible/stretchable electronics have imposed a new challenge for adhesives: to bind the various components of a sophisticated system in a flexible/stretchable manner. Applications include flexible displays,[2−4] stretchable touch panels,[5] foldable screens,[6] skin electronics,[7] implantable medical devices,[8] and soft robotics.[9] Existing polymeric adhesives, such as the quintessential pressure-sensitive adhesives (PSAs),[10] are readily soft and stretchable; however, their prominent viscoelastic nature severely hampers their uses in engineering practices where prolonged static/dynamic deformations are expected. For example, residual strain accumulates under cyclic stretching to cause buckling,[11] slow relaxation gives rise to a substantial level of residual stress,[12] which is often the culprit of surface cracking[13] and stress corrosion,[14] and the strain mismatch between the adhesive and adherend leads to wrinkling.[15] Whereas intense efforts have been devoted recently to developing adhesives with mitigated viscoelasticity,[12,16−23] previous works have mostly employed monolithic polymer networks which inevitably compromise between two contradictory properties: i.e., hyperelasticity and adhesiveness. Although subtle microstructures have been constructed on the surface of hyperelastic elastomers,[24−27] their microfabrication is complex, time-consuming, and difficult to scale up.

The conflict between hyperelasticity and adhesiveness is inherent in a homogeneous polymer network. Hyperelasticity is a bulk property and relates to the reversible change of the entropy of polymer chains,[28] which dictates that the change in the configuration of the polymer chain takes place without a dissipative process such as intermolecular friction. In comparison, the adhesiveness of a polymer network is mostly a surface property and relates to intermolecular interactions.[29] The polymer chains on the surface must interact strongly with the surface of the adherend to engender a relatively high interfacial adhesion, Γ_s, so as to maintain the cohesion of the adhesive−adherend interface, which is pivotal for effectively transferring a large deformation into the bulk of the adhesive and/or the adherend to elicit energy dissipation, Γ_b. The sum of Γ_s and Γ_b determines the apparent adhesion energy for the adhesive.[30] As illustrated in Figure 1A, in general, a hyperelastic polymer network is highly cross-linked such that

Received: July 15, 2022
Accepted: October 3, 2022

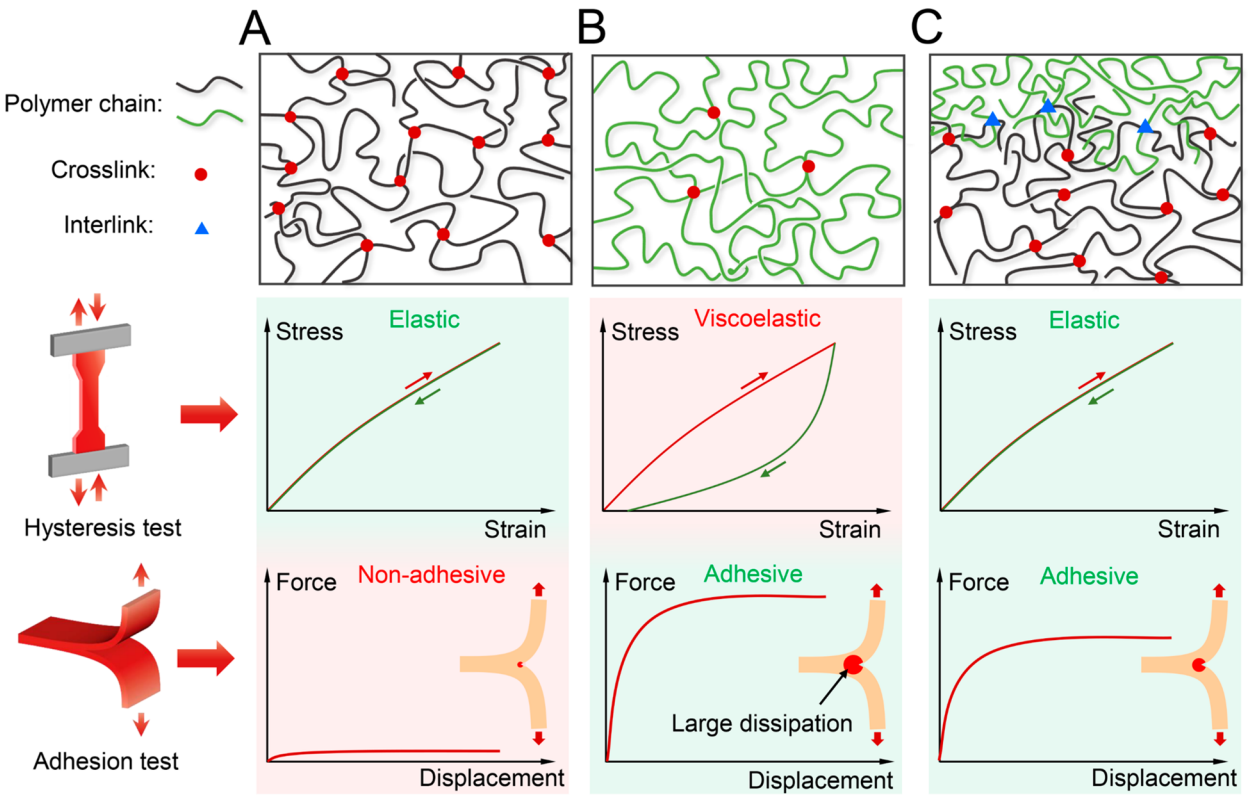

Figure 1. Schematics of various polymer networks. (A) A highly cross-linked polymer network of short chains. The network is hyperelastic in the bulk but nonadhesive at the interface, showing negligible hysteresis but low adhesion energy. (B) A loosely cross-linked polymer network of long chains. The network is adhesive at the interface but viscoelastic in the bulk, showing high adhesion energy but enormous hysteresis. (C) A heterogeneous polymer network with short chains in the bulk and long chains at the interface. The network is hyperelastic in the bulk and adhesive at the surface, showing negligible hysteresis and high adhesion energy. The surface polymers can be interlinked robustly to the bulk polymers via covalent/physical bonds (blue triangles) and/or topological entanglements.

the number of polymer chains per unit volume is large and the length of the polymer chain between two cross-links is short (Figure 1A). Entropic elasticity predominates in such a polymer network, which is hyperelastic in the bulk but nonadhesive at the interface. In cyclic tension, the stress−strain curves almost coincide, showing negligible hysteresis. In T-peeling, the nonadhesive surface cannot bear high stress and only activates a small fracture process zone in front of the crack tip, rendering a low adhesion energy. In contrast, a viscoelastic polymer network is loosely cross-linked or even just physically entangled. The number of polymer chains per unit volume is small, and the polymer chains are long (Figure 1B). Viscoelasticity prevails due to time-dependent molecular processes such as the release of chain entanglements or the relaxation of dangling chains.[31] Such a polymer network is adhesive at the interface but viscoelastic in the bulk, showing high adhesion energy but enormous hysteresis. In this sense, it is inexpedient to resolve the hyperelasticity−adhesiveness conflict based on monolithic polymer networks. The need for a general strategy for the design and synthesis of hyperelastic adhesives is urgent for the field yet remains unmet.

Here we report a strategy to resolve the conflict by designating hyperelasticity and adhesiveness to the bulk polymers and the surface polymers, respectively (Figure 1C). The resulting heterogeneous polymer network is stretchable and resilient, yet sticky, and will be termed a hyperelastic adhesive (HEA). In a HEA, the bulk polymers are highly cross-linked to be resilient and the surface polymers are loosely cross-linked to be sticky. The bulk is much thicker than the surface to dominate the hyperelastic characters. The surface polymers are interlinked robustly to the bulk polymers to invoke the elastic dissipater mechanism for elevated adhesion energy.[32] Such robust interlinks can be achieved via covalent/physical bonds and/or topological entanglements. To demonstrate the proposed principle, we select the acrylate polymers and synthesize a series of HEAs, with the optimized version showing a hysteresis as low as 4% at 100% strain and an adhesion energy of 270 J m^{-2}. The HEA is optically transparent, thermally stable, and spontaneously adhesive to diverse solids, including ceramic, glass, metal, elastomer, plastic, and wood. Within the reliability paradigm, HEA exhibits stability superior to the viscoelastic adhesive counterparts against cyclic load, relaxation, and creep. The unique combination of hyperelasticity and adhesiveness enables novel applications, such as ionic sensors with highly stable electrical performances and rapid response and recovery speed and lamellar structures with suppressed wrinkling under cyclic bending. The general design strategy of the HEA opens ample space not only to investigations of the fundamentals of soft adhesives in physics, chemistry, and materials science but also to practical applications of stretchable and resilient adhesives across various fields.

RESULTS AND DISCUSSION

The working principle of a HEA requires two distinct polymer networks: one hyperelastic and the other adhesive. We select the acrylate polymers for exemplification, with the chemical

https://doi.org/10.1021/acsami.2c12658
ACS Appl. Mater. Interfaces XXXX, XXX, XXX−XXX

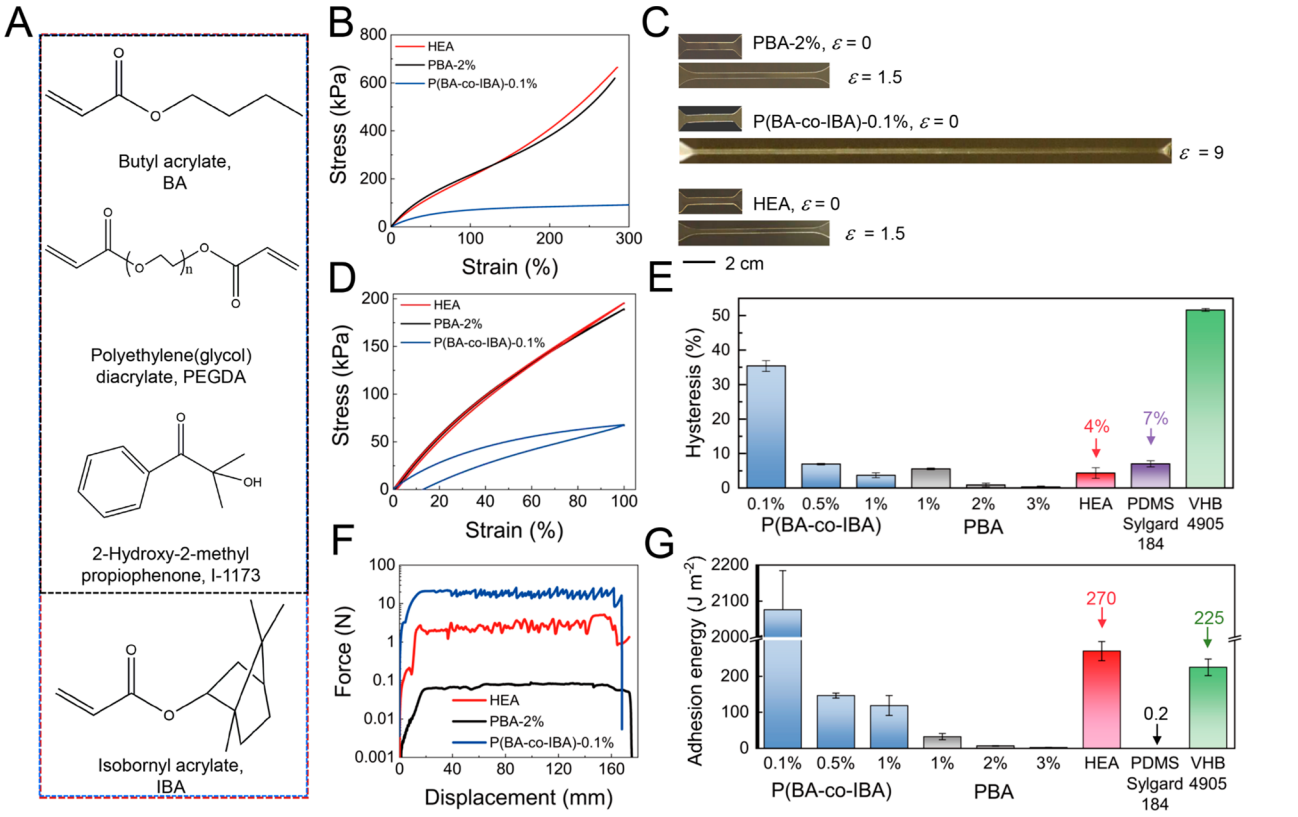

Figure 2. Synthesis and optimizations of HEA. (A) Chemical structures of the ingredients for the synthesis of a hyperelastic nonadhesive PBA network (black dashed frame), a viscoelastic adhesive P(BA-*co*-IBA) network (blue dashed frame), and a HEA network consisting of hyperelastic PBA bulk and adhesive P(BA-*co*-IBA) surface (red dashed frame). (B) Nominal stress−strain curves of HEA, PBA-2%, and P(BA-*co*-IBA)-0.1%. (C) Photos of dumbbell-shaped samples of PBA-2%, P(BA-*co*-IBA)-0.1%, and HEA at different strains as indicated. (D) Cyclic load−unload curves of HEA, PBA-2%, and P(BA-*co*-IBA)-0.1%. (E) Hystereses of various polymer networks. (F) Peel force−displacement curves of HEA, PBA-2%, and P(BA-*co*-IBA)-0.1%. (G) Adhesion energies of various polymer networks.

structures of the ingredients being given in Figure 2A. For the hyperelastic bulk, butyl acrylate (BA), polythylene(glycol) diacrylate (PEGDA), and 2-hydroxy-2-methylpropiophenone (Irgacure 1173) are used as the monomer, cross-linker, and photoinitiator, respectively, to synthesize a homopolymer poly(butyl acrylate) (PBA) network. The hyperelastic characters of PBA can be tuned via adjusting the amount of PEGDA. PBA-*x*% means that the weight percentage of PEGDA with respect to BA is *x*%. For the adhesive surface, isobornyl acrylate (IBA), 20 wt %, is added in addition to the ingredients used for PBA to form a random copolymer poly(butyl acrylate-*co*-isobornyl acrylate) (P(BA-*co*-IBA)) network. Similarly, the adhesive characters of P(BA-*co*-IBA) can be tuned via adjusting the amount of PEGDA, and P(BA-*co*-IBA)-*y*% means that the weight percentage of PEGDA with respect to the total weight of monomer is *y*%. In addition, the adhesive characteristics of P(BA-*co*-IBA) can also be tuned by varying the molar ratio between BA and IBA,[33] since the steric hindrance effects of the pendant side group of IBA facilitate the formation of network defects: e.g., dangling chains.[34] The thicknesses of the bulk and surface of the resulting HEA are about 1 mm and 50 μm, respectively.

We first characterize the properties of PBA and compare with those of a highly elastic silicone elastomer, polydimethylsiloxane (PDMS, Sylgard 184, curing ratio 10/1) (Figure S1). Uniaxial tension shows that PBA-1% and PBA-2% are more stretchable and softer than PDMS. The hystereses of all PBAs tested, of 5.6%, 0.9%, and 0.3% for PBA-1%, PBA-2%, PBA-3%, respectively, are lower than that of PDMS, 7%. T-peeling tests give adhesion energies, calculated by $\Gamma = 2F_{ss}/w$,[35] where F_{ss} is the steady-state peel force and w the width of sample, of 23.4, 6.44, 3.00, and 0.20 J m^{-2} for PBA-1%, PBA-2%, PBA-3%, and PDMS, respectively. We then characterize the properties of P(BA-*co*-IBA) and compare with those of VHB 4905 (3M), a commercially available and widely used soft, stretchable, and transparent acrylate adhesive (Figure S2). Both P(BA-*co*-IBA) and VHB are highly stretchable and show pronounced hysteresis. The adhesion energies are 2028, 151, 97, and 225 J m^{-2} for P(BA-*co*-IBA)-0.1%, P(BA-*co*-IBA)-0.5%, P(BA-*co*-IBA)-1%, and VHB 4905, respectively.

Now that we have a group of hyperelastic polymer networks and a group of adhesive polymer networks, we seek to synthesize and optimize HEAs with tactfully combined hyperelasticity and adhesiveness. Specifically, we select PBA-2% for the bulk and P(BA-*co*-IBA)-0.1% for the surface. We use a two-step method: synthesize a hyperelastic PBA-2% andthen coat it with a thin layer of P(BA-*co*-IBA)-0.1%. Targeting low hysteresis and high adhesion energy, we optimize the synthetic conditions (Figures S3 and S4) and optimally set the precuring time of P(BA-*co*-IBA)-0.1% as 1 min. The resulting HEA has a bulk/surface thickness ratio of 10/1. Moreover, the effects of additional UV illumination on the bulk properties of PBA-2% (Figure S5) and the effects of copolymerization of IBA and the content of PEGDA on the adhesion of the HEA (Figure S6) are also examined.

https://doi.org/10.1021/acsami.2c12658
ACS Appl. Mater. Interfaces XXXX, XXX, XXX−XXX

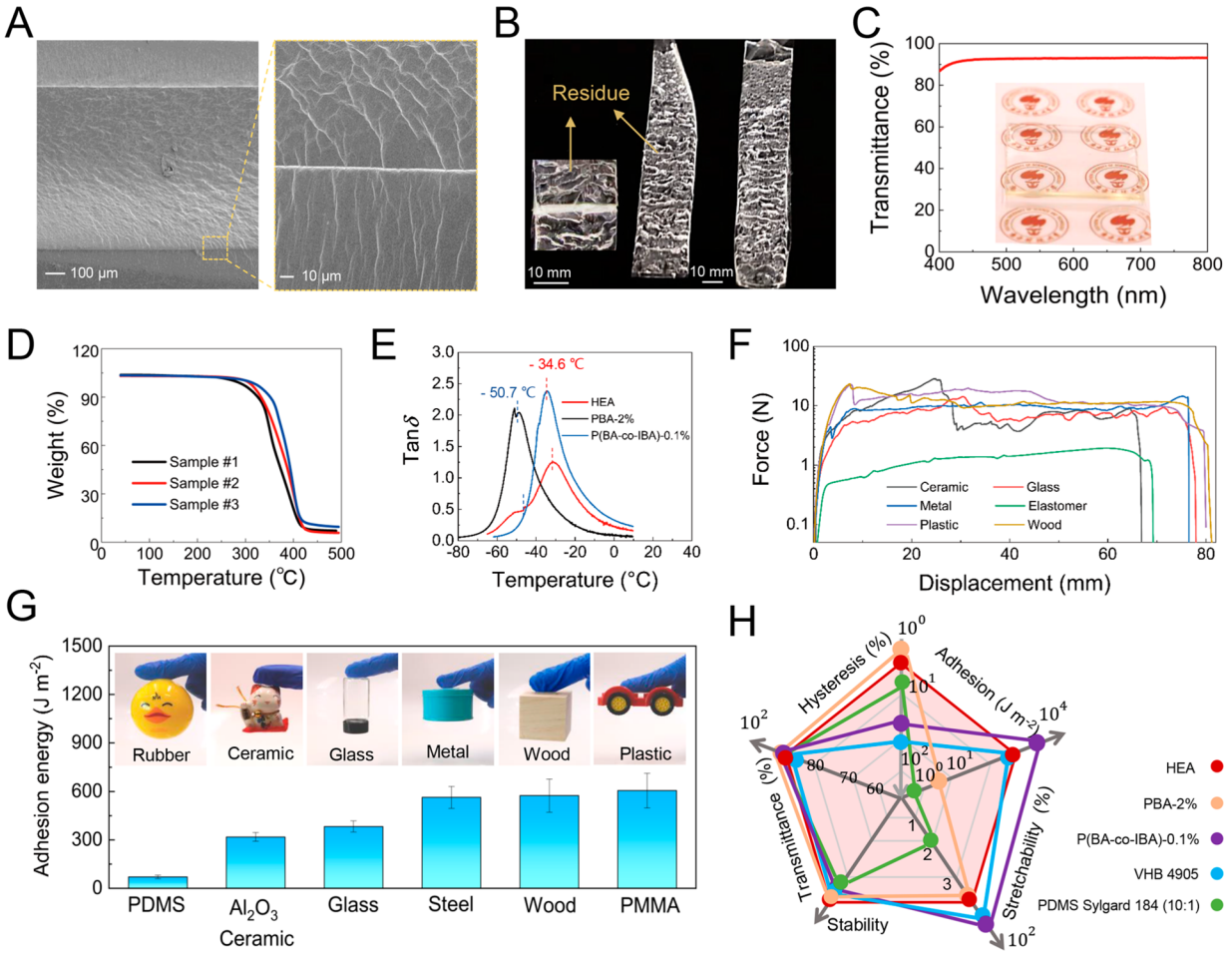

Figure 3. Characterizations of HEA. (A) Scanning electron microscopic images showing the lamellar structure composed of a layer of PBA-2% sandwiched by two layers of P(BA-*co*-IBA)-0.1%. (B) Images showing the cohesive failure of HEA during and after 180° peeling. (C) Transmittance against wavelength in the range of 400−800 nm. The inset shows a piece of HEA placed on a sheet of paper printed with logos. (D) Thermogravimetric analysis from 40 to 500 °C. (E) Glass transition temperature measurements of HEA, PBA-2%, and P(BA-*co*-IBA)-0.1%. (F) 90° peel force−displacement curves of HEA on various substrates. Al_2O_3 ceramic, silica glass, stainless steel, PDMS elastomer, PMMA plastic, and basswood are used. (G) Adhesion energy of HEA on various substrates. The inset photos illustrate the adhesion of HEA to different objects. (H) Property chart of various materials.

Next, we characterize the performances of as-prepared HEAs. The uniaxial tensile stress−strain curve of HEA is expectedly comparable to that of PBA-2%, while P(BA-*co*-IBA)-0.1% is softer and more stretchable (Figure 2B), with their mechanical properties being summarized and compared in Table S1. Figure 2C showcases the dumbbell-shaped samples of HEA, PBA-2%, and P(BA-*co*-IBA)-0.1% at undeformed and deformed states with various strains as indicated. In the hysteresis tests with 100% strain, HEA and PBA-2% show tiny loops while P(BA-*co*-IBA)-0.1% shows a pronounced loop (Figure 2D). The hystereses of various polymer networks are compared in Figure 2E. In particular, the hysteresis of HEA, 4%, is even lower than that of PDMS, 7%. The hysteresis of HEA is almost independent of the maximum strain (Figure S7). In cyclic tension with progressively increased maximum strain, HEA and PBA-2% are highly resilient while P(BA-*co*-IBA)-0.1% exhibits the Mullins effect (Figure S8). Moreover, the mechanical responses of the HEA barely change as the strain rate varies from 0.0125 to 0.1 s^{-1}, again manifesting the hyperelasticity of the HEA (Figure S9). In addition, the time and temperature dependences of the HEA and its constituents are further studied and compared (Figures S10 and S11), which indicate prominent linear viscoelasticity. In T-peeling tests, the plateaued peel force of the HEA is larger than that of PBA-2% but smaller than that of P(BA-*co*-IBA)-0.1% (Figure 2F). Nevertheless, the adhesion energy of HEA, 270 J m^{-2}, is still higher than that of VHB 4905, 225 J m^{-2} (Figure 2G). Recall that the HEA has a total thickness of 1.1 mm with a bulk/surface thickness ratio of 10/1. In general, the total thickness does not affect the hyperelasticity, i.e. hysteresis, while the total thickness affects the adhesiveness of the HEA. Adhesion energy is positively related to the size of the fracture process zone during the peel test. The size of the fracture process zone is a material parameter and scales with the fractocohesive length, defined as the ratio of the fracture toughness over the work of the fracture.[36] When the characteristic length of the sample (the thickness of P(BA-*co*-IBA)-0.1% in the case of the HEA) is smaller than the fractocohesive length, the thicker the sample, the larger the adhesion energy. When the characteristic length of the sample is larger than the fractocohesive length, the adhesion energy becomes independent of the thickness.[32] We have synthesized HEAs with a 2 mm PBA-2% bulk and an ~300 μm P(BA-*co*-IBA)-0.1% surface layer. The thicker HEA

https://doi.org/10.1021/acsami.2c12658
ACS Appl. Mater. Interfaces XXXX, XXX, XXX−XXX

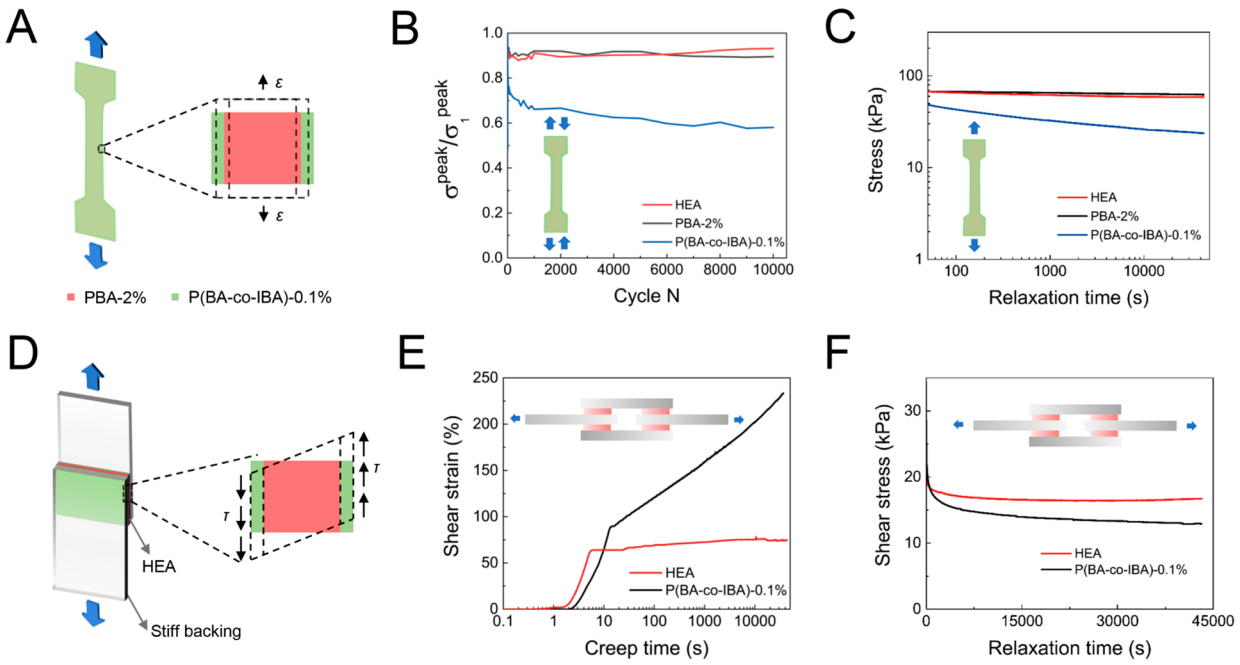

Figure 4. Stability of HEA. (A) Schematic of HEA subjected to a tensile strain ε. (B) Ratio of σ^{peak} over σ_1^{peak} as a function of the number of cycles, where σ^{peak} and σ_1^{peak} are the peak stresses at 100% strain of a certain cycle and of the first cycle, respectively. (C) Relaxation tests with tensile strains of 25% for HEA and PBA-2% and 50% for P(BA-*co*-IBA)-0.1%. (D) Schematic of the HEA subjected to a lap shear of stress magnitude τ. (E) Creep test of HEA and P(BA-*co*-IBA)-0.1% under a shear stress of 50 kPa. (F) Relaxation of HEA and P(BA-*co*-IBA)-0.1% with a shear strain of 100%.

exhibits a hysteresis of 6.7% and an adhesion energy of 400 J m^{-2}. The higher adhesion energy of thicker HEA implies that the fractocohesive length of P(BA-*co*-IBA)-0.1% is greater than its thickness.

The HEA possesses a lamellar structure with sharp interfaces (Figure 3A). These interfaces need to be robust to avoid premature interfacial failure and to effectively elicit bulk dissipation in PBA-2% and P(BA-*co*-IBA)-0.1%. Notably, the similarity of the chemistries of PBA and P(BA-*co*-IBA) facilitates the formation of a robust interface through topological entanglements such that, during the peel, a cohesive fracture propagates along the PBA layer (Figure S12) instead of the interface between PBA and P(BA-*co*-IBA) in the HEA (Figure 3B). Soft and stretchable adhesives are frequently used in assembling optoelectronic devices such as display panels, where optical transparency and tolerance over a wide temperature range can be vital. In this regard, the HEA is highly transparent to meet the requirement, with an average transmittance of 91% in the range of 400−800 nm (Figure 3C). Thermogravimetric analysis scanning from 40 to 500 °C reveals that the HEA is stable up to 250 °C (Figure 3D). In the low-temperature regime, HEA is stable down to −34.6 °C, and a second glass transition temperature, −50.7 °C, is detected (Figure 3E). The two temperatures correspond to the constituents of PBA-2% and P(BA-*co*-IBA)-0.1%, respectively (Figure S13). The wide temperature range should fulfill the requirements of many engineering applications. The loss factor of HEA is smaller than that of P(BA-*co*-IBA)-0.1% because the HEA is more elastic at the T_g value of P(BA-*co*-IBA)-0.1%. The loss factor of HEA is also smaller than that of PBA-2% because at the T_g value of PBA-2%, which is much lower than the T_g value of P(BA-*co*-IBA)-0.1%, P(BA-*co*-IBA)-0.1% can be even more elastic than PBA-2%.

The adhesion of the HEA relies on the physical interactions between the loosely cross-linked long P(BA-*co*-IBA)-0.1% polymers and the surface of the adherend, so that spontaneous and strong adhesion is anticipated on various substrates. We perform 90° peeling tests on different materials, including ceramic, glass, metal, elastomer, plastic, and wood (Figure 3F), and compare their adhesion energies, calculated as $\Gamma = F_{ss}/w$, in Figure 3G. Because the IBA and BA segments are both polar, the HEA adheres more strongly to polar substrates than to nonpolar substrates. Yet, despite the dissimilarity of chemistry between HEA and PDMS, an adhesion energy of ∼130 J m^{-2} is still achieved. The inset photos demonstrate the versatility of objects that can be pasted on and lifted up by HEA. Unlike common PSAs,[37,38] the contact time does not profoundly affect the adhesion energy of HEAs (Figure S14). We summarize the properties of the HEA, including stretchability, adhesion, hysteresis, transmittance, and stability, and compare with those of its parent materials, as well as PDMS and VHB 4905 in the property chart (Figure 3H). Notably, the HEA exhibits marvelous all-round properties.

During its lifespan, an adhesive often needs to carry prolonged static/cyclic loads. We probe the long-term stability of the HEA using uniaxial tension and shear. First, we apply uniaxial tension with a prescribed strain (Figure 4A). Under a cyclic load with a maximum strain of 100%, the stress−strain curves of the HEA stabilize over 10000 cycles (Figure S15). We plot the ratio of the peak stress of a certain cycle σ^{peak} over the peak stress of the first cycle σ_1^{peak} as a function of cycle number (Figure 4B). The ratio remains mostly unchanged for HEA and PBA-2% while it gradually decreases for P(BA-*co*-IBA)-0.1%. In the relaxation test, the stresses of the HEA and PBA-2% hold steady while the stress of P(BA-*co*-IBA)-0.1% keeps decreasing (Figure 4C). Second, we apply a lap-shear test with a prescribed shear stress (Figure 4D). A monotonic

https://doi.org/10.1021/acsami.2c12658
ACS Appl. Mater. Interfaces XXXX, XXX, XXX−XXX

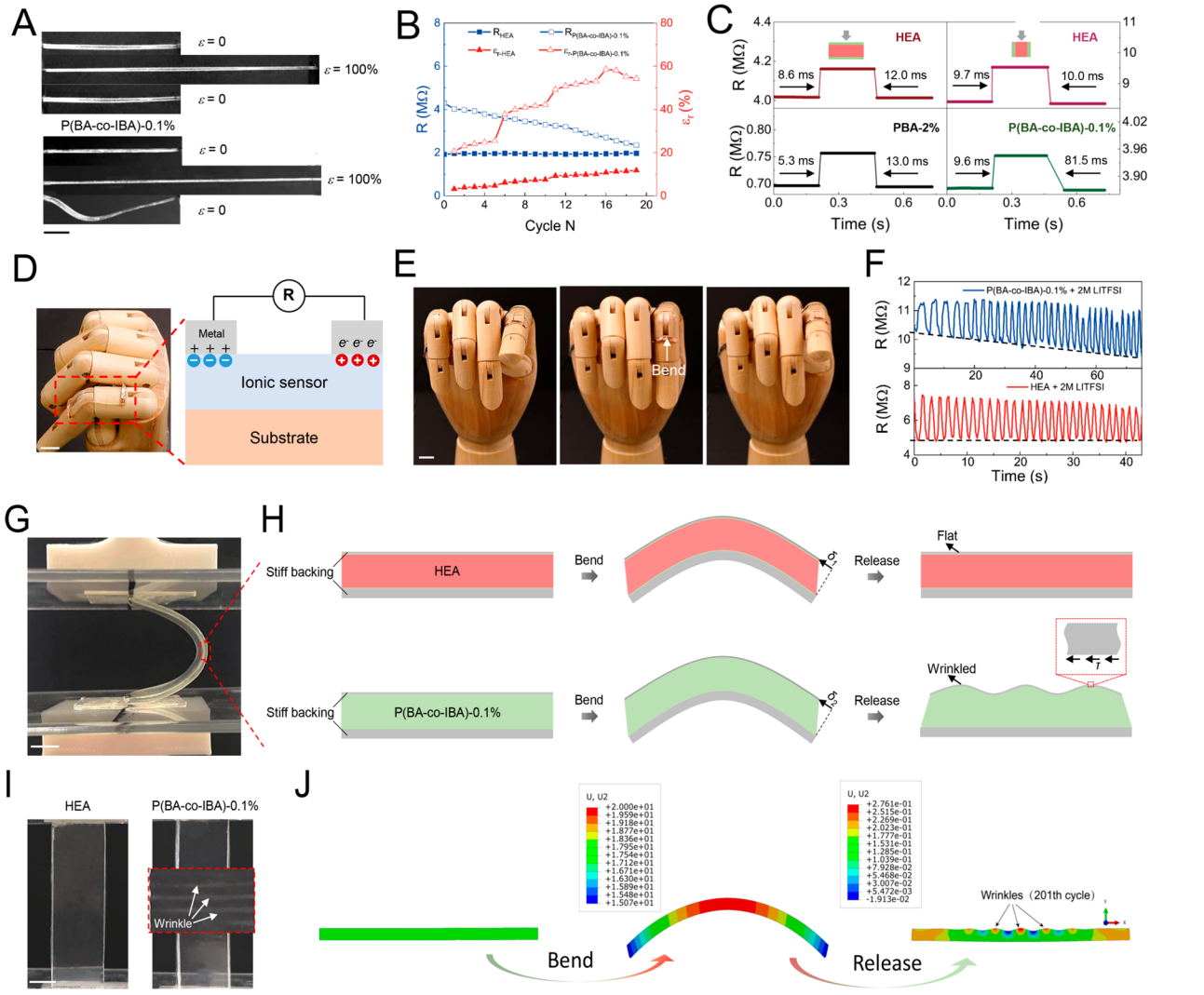

Figure 5. Applications of HEA. (A) Sequential images showing the residual deformation of ionic HEA and P(BA-*co*-IBA)-0.1%. (B) Baseline resistance and residual strain as a function of the number of cycles. (C) Response and recovery times of ionic HEA, PBA-2%, and P(BA-*co*-IBA)-0.1%. (D) Hyperelastic adhesive ionic sensor adhering to a robotic index finger with the working principle schematized. (E) Images showing the original state, the bent state, and the recovered state of the robotic index finger, during which the ionic sensor adapts well to the deformation. (F) Continuous resistance monitoring of ionic P(BA-*co*-IBA)-0.1% and ionic HEA attached on a robotic index finger. (G) Lamellar structure consisting of a layer of HEA sandwiched between two PET films being compressed to bend. (H) Schematic illustrating the deformation process of the lamellar structures with HEA (top) and P(BA-*co*-IBA)-0.1% (bottom). (I) Images showing the wrinkle-free lamellar structure with the HEA and the wrinkled lamellar structure with P(BA-*co*-IBA)-0.1% after 1000 cycles of bending. (J) Simulation results of the repeated bending of the lamellar structure with P(BA-*co*-IBA)-0.1% at the 201st cycle.

lap-shear test is performed to obtain the shear strength, ~200 kPa, and the shear strain to rupture, ~300% (Figure S16). Under a creep test with a shear stress of 50 kPa, the shear strain of HEA goes up slightly and then plateaus while the shear strain of P(BA-*co*-IBA)-0.1% keeps upshifting (Figure 4E). We further measure the creep recovery time, defined as the time to regain 80% of deformation. We apply a stress of 50 kPa, hold it for 100 s, then unload to zero force while we keep recording the strain for 3 min and obtain about 16.2 s for the HEA and about 48.6 s for P(BA-*co*-IBA)-0.1% (Figure S17). In a relaxation test with a shear strain of 50%, the shear stress of the HEA drops somewhat and then stabilizes while the shear stress of P(BA-*co*-IBA)-0.1% keeps going down (Figure 4F).

The stability of the HEA is understood as follows. The hyperelastic PBA-2% can be modeled as a spring, and the viscoelastic P(BA-*co*-IBA)-0.1% can be described by the Zener model. Under uniaxial tension, PBA-2% and P(BA-*co*-IBA)-0.1% are in parallel (Figure S18). Since the modulus (378.6 kPa) and the thickness (1 mm) of PBA-2% are larger than those of P(BA-*co*-IBA)-0.1% (191.4 kPa and 0.1 mm), the mechanical responses of the HEA are dominated by the hyperelastic PBA-2%. For example, the stiffness of HEA is $E_{HEA}h_{HEA} = E_{PBA}h_{PBA} + E_{P(BA\text{-}co\text{-}IBA)}h_{P(BA\text{-}co\text{-}IBA)} \approx E_{PBA}h_{PBA}$. In the lap-shear scenario, PBA-2% and P(BA-*co*-IBA)-0.1% are in series (Figure S19). When it is subjected to a step constant shear stress, the PBA-2% layer barely creeps. While the P(BA-*co*-IBA)-0.1% layer may creep somewhat, the creep displacement is small due to the thin thickness, the covalent cross-links, and the robust interfacial interlinks. Likewise, the PBA-2% layer relaxes negligibly but the P(BA-*co*-IBA)-0.1% layer relaxes under a constant shear strain.

We further characterize the stability of the HEA under harsh conditions. The HEA maintains high optical transparency at a high relative humidity of 95% for 24 h, at either 25 or 60 °C

https://doi.org/10.1021/acsami.2c12658
ACS Appl. Mater. Interfaces XXXX, XXX, XXX−XXX

(Figure S20). Strong adhesion is preserved at both high (60 °C) and low (−20 °C) temperatures (Figure S21). Under a cyclic fatigue fracture test, the HEA exhibits an interfacial fatigue threshold of 25 J m^{-2} (Figure S22). The fatigue threshold can be theoretically estimated by invoking the Lake−Thomas model.[39] Dropping off the dimensionless prefactor, the Lake−Thomas theory predicts that the fatigue threshold of a polymer network is $\Gamma_o = JLn^{0.5}/V$, where J is the bond energy, L the length per repeat unit, n the number of repeat units between two cross-links, and V the volume of the repeat unit. In our experiments, representative values are $J = 3.3 \times 10^{-19}$ J, $V = M_{monomer}/\rho N_A = 2.6 \times 10^{-28}$ m^3, $L = 0.447$ nm, and $n = n_{monomer}/2n_{PEGDA} = 2170$, where $M_{monomer}$ is the molar mass of monomer, ρ is the density, N_A is Avogadro's constant, $n_{monomer}$ is the number of monomers and n_{PEGDA} is the number of PEGDAs. With these, we estimate the fatigue threshold to be 26.4 J m^{-2}, which agrees well with experiment.

The unique combination of hyperelasticity and adhesiveness enables new functionalities that have been previously inaccessible for monolithic polymer networks. For example, together with the merits of low dielectric constant and dissipation factor (Figure S23, Table S2), the HEA promises potential applications as an insulating adhesive for soft electronics. As another example, ionic sensors need not only to be soft and stretchable to accommodate deformation but also to be adhesive to firmly anchor on the object monitored.[40] Nevertheless, in addition to the lack of adhesiveness, most stretchable ionic sensors exhibit prominent residual strains, causing significant shifts of the baseline resistance which are detrimental to applications. Here we synthesize a stretchable, resilient, and adhesive ionic sensor by incorporating lithium bis(trifluoromethanesulfonyl)imide (LiTFSI) into the matrix of the HEA,[41] without severely altering the mechanical properties (Figure S24). An electrochemical impedance spectroscopy (EIS) measurement gives an ionic conductivity of 6.5×10^{-4} S cm^{-1} (Figure S25). As shown in Figure 5A, after being elongated to a strain of 100% and then released, the ionic HEA recovers its original shape well, while a large residual strain persists in the ionic P(BA-*co*-IBA)-0.1% such that the sample even buckles. Under a consecutive load−unload tensile test with maximum strains of 50%, 100%, 150%, and 200%, each repeated five times, the ionic HEA has a mostly constant baseline resistance and a slight increase in residual strain, while the ionic P(BA-*co*-IBA)-0.1% keeps shifting its baseline resistance and residual strain (Figure 5B). We evaluate the dynamic response/recovery speed of different ionic sensors by knocking a 20 g weight on the sensor (Figure 5C). Whereas the response times are all shorter than 10 ms, the recovery speed of ionic P(BA-*co*-IBA)-0.1%, ∼81.5 ms, is much slower than those of ionic PBA-2%, ∼10 ms, and ionic HEA, in either parallel or serial mode. We demonstrate the application of ionic HEA as a resistive sensor for continuously monitoring the motion of a robotic finger (Figure 5D). The strong adhesion ensures that the ionic HEA adheres firmly to the robotic finger during deformation (Figure 5E). Under cyclic bending, the baseline resistance of ionic P(BA-*co*-IBA)-0.1% keeps changing over time, while the baseline resistance of ionic HEA is stable (Figure 5F). Note that a change in the transparency of the ionic sensor upon stretching is important for wearable applications. For the HEA, the transmittance decreases, for instance, from ∼92.3% at 0% strain to ∼87.8% at 50% strain at 500 nm, which can be attributed to the crystallinity caused by the alignment of the polymer chains.[11,42]

As another example, we demonstrate the uses of HEA for assembling thin laminates. Such a scenario of using soft adhesives to assemble multiple layers of distinct mechanical properties is becoming pervasive, for instance, in the flexible/stretchable screens of portable devices,[12,20,21] whereby repeated deformation is unavoidable. However, the existing optically clear adhesives, adhered to adherends of much higher modulus, suffer from creep over repeated deformations, resulting in an interfacial fracture or wrinkling,[15] both of which dramatically deteriorate the optical performances of the devices. Here we mitigate this issue by using the HEA. Without losing generality, we fabricate a laminate sample by sandwiching a layer of HEA with two layers of PET films, with thicknesses of 25 and 200 μm, and bend it through lateral compression from the two edges (Figure 5G). Subjected to bending, the adhesive layer shears significantly, and conspicuous sliding occurs between the two PET layers (Figure S26). After releasing, the HEA can spring back rapidly whereas a viscoelastic adhesive such as P(BA-*co*-IBA)-0.1% cannot, exerting in-plane compression to the thinner PET film. As a result, the HEA laminate will remain flat, while that with P(BA-*co*-IBA)-0.1% will wrinkle (Figure 5H). We verify the above hypothesis by carrying out cyclic bending with a radius of curvature of ∼2 cm. As expected, the structure with HEA remains flat while wrinkles gradually appear in the lamellar structure with P(BA-*co*-IBA)-0.1% after cyclic bending (Figure 5I). Furthermore, we conduct a finite element simulation to analyze the wrinkling process under a plane-strain condition, by modeling the P(BA-*co*-IBA)-0.1% layer as a viscohyperelastic and the PET layers as a linear elastic, with the material parameters being obtained from experiments. Shear of the viscoelastic layer accumulates with the cycles of bending, resulting in the relative sliding of the PET layers and an inhomogeneous stress distribution (Figure S27). Eventually, wrinkles form due to the in-plane compression in the thinner PET film (Figure 5J).

CONCLUSION

In summary, we report a design strategy to synthesize stretchable and resilient adhesives by decoupling the hyperelasticity and the adhesiveness in a heterogeneous polymer network. The resulting HEA possesses a low hysteresis of 4% at 100% strain and a high adhesion energy of 270 J m^{-2}. Excellent optical transparency, thermal stability, and nonspecificity as well as long-term stability against cyclic fatigue, relaxation, and creep are manifested. We demonstrate two applications enabled by the unique combination of the marked performances of the HEA. The proposed principle of the HEA is simple and generic. The design and synthesis of HEAs with various attributes provide plentiful possibilities for broad engineering applications.

MATERIALS AND METHODS

Materials. All chemicals were purchased and used without further purification. Butyl acrylate (BA; Macklin, C12617411) and isobornyl acrylate (IBA; Aladdin, K2019110) were used as monomers. Polyethylene(glycol) diacrylate (PEGDA-600; Shanghai D&B Biological Science and Technology Co. Ltd., China) and Irgacure-1173 (I-1173; Aladdin, H110280) were used as the cross-linker and photoinitiator, respectively. Benzophenone (BP; Aladdin, L1917127) was used as a hydrogen-stripping photoinitiator for surface treatment. Lithium bis(trifluoromethanesulfonyl)imide (LiTFSI; Aladdin, H2118038) salt was used for ionic conductivity. For commercial elastomers, polydimethylsiloxane (PDMS) Sylgard 184 from Dow

https://doi.org/10.1021/acsami.2c12658
ACS Appl. Mater. Interfaces XXXX, XXX, XXX−XXX

Corning was synthesized with a weight ratio (base over cross-linking agent) of 1/10 at 65 °C for 4 h. The acrylate adhesive VHB 4905 was purchased from 3M company, whose glass transition temperature (T_g) value is −40 °C; its time-dependent properties are characterized in Figure S28.

Synthesis of Materials. *PBA-x%.* Monomer BA, cross-linker PEGDA, and photoinitiator I-1173 were mixed to form a homogeneous precursor. The mass percentages, with respect to BA, were fixed at 1 wt % for I-1173 and varied from 1 to 5 wt % for PEGDA. Then, the precursor was injected into a glass mold, which was spaced by a 1 mm thick spacer, and cured under ultraviolet light (365 nm, 30 W) for 30 min at room temperature. The surfaces of the glass mold were coated with release films for easy demolding.

Synthesis of P(BA-co-IBA)-y%. The monomers BA and IBA (mass ratio with respect to BA was 1/4), PEGDA as a cross-linker, and photoinitiator I-1173 as were mixed to form a homogeneous precursor. The mass percentages, with respect to monomer, were fixed at 0.1 wt % for I-1173 and varied from 0.1 to 1 wt % for PEGDA. Then, the precursor was injected into a glass mold, which was spaced by a 1 mm thick spacer, and cured under ultraviolet light (365 nm, 30 W) for 30 min at room temperature. The surfaces of the glass mold were coated with release films for easy demolding.

Synthesis of the HEA. HEA was synthesized in two steps: we prepared the hyperelastic PBA-2% (corresponding to a cross-linker/monomer molar ratio of 0.43%) and then coated it with thin layers of P(BA-*co*-IBA)-0.1% (corresponding to a cross-linker/monomer molar ratio of 0.023%). The resulting cross-link densities are about 0.015 and 0.0086, respectively, for PBA-2% and P(BA-*co*-IBA)-0.1%, provided that the molecular weight between two cross-links can be calculated using the equation $M_c = RT\rho/G'$, where M_c is the molecular weight, R is the universal gas constant, 8.314 J K^{-1} mol^{-1}, T is the absolute temperature, ρ is the density of the polymer, and G' is the plateaued storage modulus measured from a rheology test (Figure S13). For coating, the precursor of P(BA-*co*-IBA)-0.1% was precured under ultraviolet light for 1 min under a nitrogen atmosphere, followed by immediate cooling to room temperature, to obtain a viscous precured solution. The prepared PBA-2% was immersed into a benzophenone solution (2 wt % in ethanol) for 2 min, dried at 65 °C for 1 min, dip-coated into the precured P(BA-*co*-IBA)-0.1% solution, and suspended in the air for 1 min. Finally, the sample was covered with two pieces of PET film and exposed to ultraviolet light (365 nm, 30 W) for 20 min. The resulting HEA had a thickness of ∼1.1 mm. The synthesis of ionic HEA was identical with the synthesis of HEA except that 2 M LiTFSI was added during the preparation of the precursor of PBA-2%.

Mechanical Characterizations. *Tensile and Hysteresis Tests.* All specimens for tensile and hysteresis tests were cut into a dumbbell shape 5 mm in width and 30 mm in gauge length using a laser cutter (Epilog, Fusion Pro 36). The samples were loaded onto a tensile machine (Instron 5966, 100 N load cell) and stretched at a loading velocity of 30 mm min^{-1} at room temperature. For cyclic tests, a fatigue testing machine (Instron E3000, 250 N load cell) was used and a force-controlled mode with a triangular loading profile with a frequency of 1 Hz was applied. Hereafter, unless otherwise specified, each mechanical characterization was repeated at least three times.

Peeling Test. To measure the adhesion energy, the specimens were cut into a rectangular shape with areal dimensions of width × length = 20 mm × 80 mm. For T-peeling, two pieces of 25 μm thick PET backings were glued on the two surfaces of the adhesive. An Instron 5966 instrument with a 100 N load cell was used for the monotonic peeling test, and an Instron E3000 instrument with a 250 N load cell, operated at a force-controlled mode with a triangular loading profile with a frequency of 1 Hz, was used for the fatigue test of adhesion. For 90° peeling, the top surface of the adhesive was glued to a layer of 25 μm thick PET backing and the bottom surface was directly attached onto the substrate. The peel velocity was fixed at 30 mm min^{-1}, and the experiments were performed at room temperature.

Lap Shear Test. For room-temperature shear, samples were cut into a square shape with a side length of 20 mm. In monotonic lap shear, a piece of adhesive was sandwiched between two pieces of 1 mm thick acrylate sheets, which were fixed on a tensile machine (Instron 5966, 10 kN load cell) and pulled at a velocity of 30 mm min^{-1}. For high- and low-temperature shear, samples were cut into a square shape with a side length of 2 mm. The tests were performed using a dynamic thermomechanical testing machine (TA, Q850, 18N load cell) with a loading velocity of 2.5 N min^{-1}.

Stress Relaxation. Stress relaxation tests were performed on an Instron 5966 instrument. For tensile stress relaxation, samples were cut into a dumbbell shape 5 mm in width and 30 mm in gauge length, stretched to a prescribed strain at a velocity of 30 mm min^{-1}, and held at that strain for 12 h. For lap shear stress relaxation, four pieces of adhesive were symmetrically adhered to four pieces of acrylate sheets, as schematized in the inset of Figure 4E, and subjected to the prescribed shear strain at a velocity of 30 mm min^{-1}. During relaxation, the force was continuously recorded.

Creep. A lap shear creep test was conducted by symmetrically adhering four pieces of adhesive to four pieces of acrylate sheets and loading the adhesives to a prescribed shear stress at a velocity of 30 N min^{-1} using a universal tensile machine (Instron 5966, 100 N load cell). The variation of strain as a function of time was continuously recorded for 12 h.

Fatigue Adhesion. A 180° peel was used to study the fatigue of adhesion (Figure S22). Cyclic loads with a triangular profile and frequency of 1 Hz were applied using an Instron ElectroPuls E3000 instrument. The difference of displacement at the maximum force between two cycles is twice the crack growth, $\Delta d = 2\Delta c$, which was directly recorded by the tensile machine. Fatigue threshold occurs when the crack no longer propagates at a steady state and the difference of displacement is almost zero.

Material Characterizations. *Transmittance.* The ∼1.1 mm thick HEA films, which were balanced under different humidity conditions, were fixed on the sample holder of a UV−vis spectrophotometer (Metasha, UV-8000). The wavelength ranged from 400 to 800 nm.

TGA. TGA was performed on a TA Instruments (Q500 TGA) apparatus with temperature scanning from 40 to 500 °C at a heating rate of 10 °C min^{-1} under an N_2 atmosphere.

Glass Transition Temperature Measurement. DA dynamic mechanical analysis was performed on a DMA machine (TA Q850), which measured the storage modulus G' and the loss modulus G'' as a function of temperature, in tension mode. The test frequency was fixed at 1 Hz, and the temperature was scanned from +10 to −80 °C at a cooling rate of −2 °C min^{-1}. Figure S15 plots the storage modulus G', the loss modulus G'', and tan δ as a function of temperature of the HEA, PBA-2%, and P(BA-*co*-IBA)-0.1%. The glass transition temperature T_g was identified at the peak of tan δ.

Electrical Characterizations. Dielectric properties were measured using a Keysight E4991B impedance analyzer from 10 MHz to 1 GHz.

Electrochemical Impedance Spectroscopy (EIS). The impedance tests were performed on an electrochemical workstation (CHI6000E, CH Instruments, Inc.) equipped with a temperature chamber. Sample sizes were 10 × 10 mm^2 with 1.1 mm thickness. The top and bottom sides of the samples were both directly fixed with stainless steel electrodes. The amplitude of the testing voltage amplitude was set at 0.5 V.

Finite Element Analysis. To better understand the evolution and distribution of stress and strain in the PET/P(BA-*co*-IBA)-0.1%/PET lamellar structure during cyclic bending, we conducted a finite element analysis using the commercial software SIMULIA Abaqus/Standard. Since the width of the sample was much greater than the thickness, we simulated the bending as a 2D plane-strain problem. The thicknesses of the top PET, the intermediate P(BA-*co*-IBA)-0.1%, and the bottom PET were set as 0.025, 1, and 0.2 mm, respectively. PET was modeled as a linear elastic material with a Young's modulus of 2 GPa and a Poisson's ratio of 0.3. P(BA-*co*-IBA)-0.1% was modeled as an incompressible viscohyperelastic material by using a neo-Hookean elasticity of modulus 100 kPa and a Prony series for viscoelasticity, with coefficients and characteristic times being obtained by fitting the relaxation curve in Figure 4c. CPE4H elements were adopted for P(BA-*co*-IBA)-0.1% and CPE4 elements for PET. Visco steps with a tolerance of 0.001 in viscoelastic strain were used in

https://doi.org/10.1021/acsami.2c12658
ACS Appl. Mater. Interfaces XXXX, XXX, XXX−XXX

the simulations. Half of the laminate was modeled by symmetry, with a displacement boundary condition being applied to the edge.

■ ASSOCIATED CONTENT

Supporting Information

The Supporting Information is available free of charge at https://pubs.acs.org/doi/10.1021/acsami.2c12658.

Additional experimental details and materials characterizations, including the optimization of cross-linker density and fabrications of PBA, P(BA-*co*-IBA), and HEA, elastic/viscoelastic properties, rheology properties, FTIR spectra, DMA testing, peel force−displacement curves at different contact times, cyclic tests, monotonic lap shear tests, and creep recovery test of the HEA, elastic/viscoelastic models of the HEA under tensile and shear conditions, transmittance at high/low temperature, lap shear tests at high/low temperature, fatigue fracture of the adhesion of the HEA, dielectric properties for all compounds, mechanical characterizations and electrochemical impedance spectroscopy (EIS) of ionic HEA, shear slip under bending, simulation of the stress distribution of the PET/P(BA-*co*-IBA)-0.1%/PET, rheology properties of VHB 4905, and a summary of the mechanical properties and dielectric properties of all compounds (PDF)

■ AUTHOR INFORMATION

Corresponding Authors

Wei Hong − *Shenzhen Key Laboratory of Soft Mechanics & Smart Manufacturing, Department of Mechanics and Aerospace Engineering, Southern University of Science and Technology, Shenzhen 518055, People's Republic of China*; Email: hongw@sustech.edu.cn

Canhui Yang − *Shenzhen Key Laboratory of Soft Mechanics & Smart Manufacturing, Department of Mechanics and Aerospace Engineering, Southern University of Science and Technology, Shenzhen 518055, People's Republic of China*; orcid.org/0000-0001-5674-834X; Email: yangch@sustech.edu.cn

Authors

Ping Zhang − *Shenzhen Key Laboratory of Soft Mechanics & Smart Manufacturing, Department of Mechanics and Aerospace Engineering, Southern University of Science and Technology, Shenzhen 518055, People's Republic of China*

Weiyu Zhou − *Shenzhen Key Laboratory of Soft Mechanics & Smart Manufacturing, Department of Mechanics and Aerospace Engineering, Southern University of Science and Technology, Shenzhen 518055, People's Republic of China*

Yunfeng He − *Shenzhen Key Laboratory of Soft Mechanics & Smart Manufacturing, Department of Mechanics and Aerospace Engineering, Southern University of Science and Technology, Shenzhen 518055, People's Republic of China*

Ziyi Xu − *Shenzhen Key Laboratory of Soft Mechanics & Smart Manufacturing, Department of Mechanics and Aerospace Engineering, Southern University of Science and Technology, Shenzhen 518055, People's Republic of China*

Maochun Li − *Department of Materials Science and Engineering, Southern University of Science and Technology, Shenzhen 518055, People's Republic of China*

Complete contact information is available at: https://pubs.acs.org/10.1021/acsami.2c12658

Author Contributions

P.Z., W.H., and C.Y. conceived the research. P.Z. and C.Y. designed the experiments. P.Z. conducted experiments and collected data. Y.H. and Z.X. participated in the discussion of experimental design and the characterizations of samples. W.Z. carried out the finite element analysis. M.L. conducted the SEM characterizations. P.Z., W.Z., Y.H., Z.X., W.H., and C.Y. analyzed the data. P.Z. and C.Y. wrote the original manuscript with input from the other authors. W.H. and C.Y. supervised the research.

Notes

The authors declare no competing financial interest.

■ ACKNOWLEDGMENTS

The work at the Southern University of Science and Technology was supported by the Science, Technology, and Innovation Commission of Shenzhen Municipality (ZDSYS20210623092005017). C.Y. acknowledges support from the Natural Science Foundation of Guangdong Province (2214050008118) and the Stable Support Plan Program of Shenzhen Natural Science Fund Grant (K21326303). W.H. acknowledges financial support from the National Natural Science Foundation of China through Grant 11972015.

■ REFERENCES

(1) Skeist, I. *Handbook of Adhesives*; Springer Science & Business Media: 2012; pp 727−735.

(2) Shi, X.; Zuo, Y.; Zhai, P.; Shen, J.; Yang, Y.; Gao, Z.; Liao, M.; Wu, J.; Wang, J.; Xu, X.; et al. Large-Area Display Textiles Integrated with Functional Systems. *Nature* **2021**, *591* (7849), 240−245.

(3) Chen, Y.; Au, J.; Kazlas, P.; Ritenour, A.; Gates, H.; McCreary, M. Flexible Active-Matrix Electronic Ink Display. *Nature* **2003**, *423* (6936), 136−136.

(4) Sugimoto, A.; Ochi, H.; Fujimura, S.; Yoshida, A.; Miyadera, T.; Tsuchida, M. Flexible Oled Displays Using Plastic Substrates. *IEEE J. Sel. Top. Quantum Electron.* **2004**, *10* (1), 107−114.

(5) Kim, C.-C.; Lee, H.-H.; Oh, K. H.; Sun, J.-Y. Highly Stretchable, Transparent Ionic Touch Panel. *Science* **2016**, *353* (6300), 682−687.

(6) Koo, J. H.; Kim, D. C.; Shim, H. J.; Kim, T. H.; Kim, D. H. Flexible and Stretchable Smart Display: Materials, Fabrication, Device Design, and System Integration. *Adv. Funct. Mater.* **2018**, *28* (35), 1801834.

(7) Chortos, A.; Liu, J.; Bao, Z. Pursuing Prosthetic Electronic Skin. *Nature materials* **2016**, *15* (9), 937−950.

(8) Choi, Y. S.; Yin, R. T.; Pfenniger, A.; Koo, J.; Avila, R.; Benjamin Lee, K.; Chen, S. W.; Lee, G.; Li, G.; Qiao, Y.; et al. Fully Implantable and Bioresorbable Cardiac Pacemakers without Leads or Batteries. *Nature biotechnology* **2021**, *39* (10), 1228−1238.

(9) Li, G.; Chen, X.; Zhou, F.; Liang, Y.; Xiao, Y.; Cao, X.; Zhang, Z.; Zhang, M.; Wu, B.; Yin, S.; et al. Self-Powered Soft Robot in the Mariana Trench. *Nature* **2021**, *591* (7848), 66−71.

(10) Creton, C. Pressure-Sensitive Adhesives: An Introductory Course. *MRS Bull.* **2003**, *28* (6), 434−439.

(11) Lee, J. H.; Park, J.; Myung, M. H.; Baek, M.-J.; Kim, H.-S.; Lee, D. W. Stretchable and Recoverable Acrylate-Based Pressure Sensitive Adhesives with High Adhesion Performance, Optical Clarity, and Metal Corrosion Resistance. *Chemical Engineering Journal* **2021**, *406*, 126800.

(12) Lee, J.-H.; Lee, T.-H.; Shim, K.-S.; Park, J.-W.; Kim, H.-J.; Kim, Y.; Jung, S. Effect of Crosslinking Density on Adhesion Performance and Flexibility Properties of Acrylic Pressure Sensitive Adhesives for Flexible Display Applications. *Int. J. Adhes. Adhes.* **2017**, *74*, 137−143.

(13) Ho, S.; Hillman, C.; Lange, F.; Suo, Z. Surface Cracking in Layers under Biaxial, Residual Compressive Stress. *J. Am. Ceram. Soc.* **1995**, *78* (9), 2353−2359.

(14) Chen, C.-J.; Lin, K.-L. Internal Stress and Adhesion of Amorphous Ni-Cu-P Alloy on Aluminum. *Thin Solid Films* **2000**, *370* (1−2), 106−113.
(15) Huang, R.; Suo, Z. Wrinkling of a Compressed Elastic Film on a Viscous Layer. *J. Appl. Phys.* **2002**, *91* (3), 1135−1142.
(16) Gower, M.; Shanks, R. Acrylic Acid Level and Adhesive Performance and Peel Master-Curves of Acrylic Pressure-Sensitive Adhesives. *J. Polym. Sci., Part B: Polym. Phys.* **2006**, *44* (8), 1237−1252.
(17) Lee, J.-H.; Lee, T.-H.; Shim, K.-S.; Park, J.-W.; Kim, H.-J.; Kim, Y. Adhesion Performance and Recovery of Platinum Catalyzed Silicone Psas under Various Temperature Conditions for Flexible Display Applications. *Mater. Lett.* **2017**, *208*, 86−88.
(18) Lee, J.-H.; Lee, T.-H.; Shim, K.-S.; Park, J.-W.; Kim, H.-J.; Kim, Y.; Jung, S. Molecular Weight and Crosslinking on the Adhesion Performance and Flexibility of Acrylic Psas. *J. Adhes. Sci. Technol.* **2016**, *30* (21), 2316−2328.
(19) Ishikawa, N.; Furutani, M.; Arimitsu, K. Pressure-Sensitive Adhesive Utilizing Molecular Interactions between Thymine and Adenine. *J. Polym. Sci., Part A: Polym. Chem.* **2016**, *54* (10), 1332−1338.
(20) Back, J.-H.; Baek, D.; Sim, K.-B.; Oh, G.-Y.; Jang, S.-W.; Kim, H.-J.; Kim, Y. Optimization of Recovery and Relaxation of Acrylic Pressure-Sensitive Adhesives by Using Uv Patterning for Flexible Displays. *Ind. Eng. Chem. Res.* **2019**, *58* (10), 4331−4340.
(21) Park, Y.; Byun, H.; Lee, J. H. Highly Stretchable and Transparent Optical Adhesive Films Using Hierarchically Structured Rigid-Flexible Dual-Stiffness Nanoparticles. *ACS Appl. Mater. Interfaces* **2021**, *13* (1), 1493−1502.
(22) Lee, J. H.; Myung, M. H.; Baek, M. J.; Kim, H.-S.; Lee, D. W. Effects of Monomer Functionality on Physical Properties of 2-Ethylhexyl Acrylate Based Stretchable Pressure Sensitive Adhesives. *Polym. Test.* **2019**, *76*, 305−311.
(23) Baek, S.-S.; Jang, S.-J.; Hwang, S.-H. Preparation and Adhesion Performance of Transparent Acrylic Pressure Sensitive Adhesives: Effects of Substituent Structure of Acrylate Monomer. *Int. J. Adhes. Adhes.* **2016**, *64*, 72−77.
(24) Baik, S.; Kim, D. W.; Park, Y.; Lee, T. J.; Ho Bhang, S.; Pang, C. A Wet-Tolerant Adhesive Patch Inspired by Protuberances in Suction Cups of Octopi. *Nature* **2017**, *546* (7658), 396−400.
(25) Baik, S.; Lee, H. J.; Kim, D. W.; Kim, J. W.; Lee, Y.; Pang, C. Bioinspired Adhesive Architectures: From Skin Patch to Integrated Bioelectronics. *Adv. Mater.* **2019**, *31* (34), No. 1803309.
(26) Bae, W. G.; Kim, D.; Kwak, M. K.; Ha, L.; Kang, S. M.; Suh, K. Y. Enhanced Skin Adhesive Patch with Modulus-Tunable Composite Micropillars. *Adv. Healthc Mater.* **2013**, *2* (1), 109−13.
(27) Liu, X.; Liu, J.; Wang, J.; Wang, T.; Jiang, Y.; Hu, J.; Liu, Z.; Chen, X.; Yu, J. Bioinspired, Microstructured Silk Fibroin Adhesives for Flexible Skin Sensors. *ACS Appl. Mater. Interfaces* **2020**, *12* (5), 5601−5609.
(28) Rubinstein, M.; Colby, R. H. *Polymer Physics*; Oxford University Press: 2003; Vols. *253−269*.
(29) Mittal, K. The Role of the Interface in Adhesion Phenomena. *Polym. Eng. Sci.* **1977**, *17* (7), 467−473.
(30) Yuk, H.; Zhang, T.; Lin, S.; Parada, G. A.; Zhao, X. Tough Bonding of Hydrogels to Diverse Non-Porous Surfaces. *Nature materials* **2016**, *15* (2), 190−196.
(31) Watanabe, H. Viscoelasticity and Dynamics of Entangled Polymers. *Prog. Polym. Sci.* **1999**, *24* (9), 1253−1403.
(32) Liu, J.; Yang, C.; Yin, T.; Wang, Z.; Qu, S.; Suo, Z. Polyacrylamide Hydrogels. Ii. Elastic Dissipater. *Journal of the Mechanics and Physics of Solids* **2019**, *133*, 103737.
(33) Li, K.; Zan, X.; Tang, C.; Liu, Z.; Fan, J.; Qin, G.; Yang, J.; Cui, W.; Zhu, L.; Chen, Q. Tough, Instant, and Repeatable Adhesion of Self-Healable Elastomers to Diverse Soft and Hard Surfaces. *Adv. Sci. (Weinh)* **2022**, *9*, No. e2105742.
(34) Jia, F.; Song, J.; Kubiak, J. M.; Onoda, M.; Santos, P. J.; Sano, K.; Holten-Andersen, N.; Zhang, K.; Macfarlane, R. J. Brush Polymers as Nanoscale Building Blocks for Hydrogel Synthesis. *Chem. Mater.* **2021**, *33* (14), 5748−5756.
(35) Rivlin, R.; Thomas, A. G. Rupture of Rubber. I. Characteristic Energy for Tearing. *Journal of polymer science* **1953**, *10* (3), 291−318.
(36) Yang, C.; Yin, T.; Suo, Z. Polyacrylamide Hydrogels. I. Network Imperfection. *Journal of the Mechanics and Physics of Solids* **2019**, *131*, 43−55.
(37) Karyu, N.; Shitajima, K.; Fujii, S.; Nakamura, Y.; Urahama, Y. Contact Time Dependence of Tack for Crosslinked Polyacrylic Pressure-Sensitive Adhesives with Two Different Molecular Structures. *Int. J. Adhes. Adhes.* **2015**, *60*, 75−82.
(38) Lee, J. H.; Lee, D. W. Contact-Induced Molecular Rearrangement of Acrylic Acid-Incorporated Pressure Sensitive Adhesives. *Appl. Surf. Sci.* **2020**, *500*, 144246.
(39) Lake, G.; Thomas, A. The Strength of Highly Elastic Materials. *Proceedings of the Royal Society of London. Series A. Mathematical and Physical Sciences* **1967**, *300* (1460), 108−119.
(40) Yang, C.; Suo, Z. Hydrogel Ionotronics. *Nature Reviews Materials* **2018**, *3* (6), 125.
(41) Shi, L.; Zhu, T.; Gao, G.; Zhang, X.; Wei, W.; Liu, W.; Ding, S. Highly Stretchable and Transparent Ionic Conducting Elastomers. *Nat. Commun.* **2018**, *9* (1), 1−7.
(42) Lim, D.; Baek, M.-J.; Kim, H.-S.; Baig, C.; Lee, D. W. Carboxyethyl Acrylate Incorporated Optically Clear Adhesives with Outstanding Adhesion Strength and Immediate Strain Recoverability for Stretchable Electronics. *Chemical Engineering Journal* **2022**, *437*, 135390.

https://doi.org/10.1021/acsami.2c12658
ACS Appl. Mater. Interfaces XXXX, XXX, XXX−XXX